Assignment 1

Computational Fracture Mechanics (WiSe2526)

Bagus Alifah Hasyim
1080232464 68

Given Data

In this section, the parameters value for the material properties, that required by the author to calculate it based on the author's Immatrikulation Nummer, will be defined accordingly. To make the calculation detailed and transparent, each parameter will be derived step by step.

$$d_1 = 4, \quad d_2 = 6, \quad d_3 = 8 \tag{1}$$

Parameter for 1st question:

- Plate length b

  $b = 2.0 + 0.1d_1 = 2.0 + 0.1 \times 4 = 2.4$ mm

- Plate width h

  $h = b(0.4 + 0.04d_2) = 2.4(0.4 + 0.04 \times 6) = 1.536$ mm

- Crack length l

  $l = b(0.05 + 0.02d_3) = 2.4(0.05 + 0.02 \times 8) = 0.504$ mm

- Applied displacement u

  $u = 0.001 + \frac{d_3}{1000}[\text{mm}] = 0.001 + \frac{8}{1000} = 0.009$ mm

Parameter for 2nd question:

- Applied displacement u $u = 0.1 + \frac{d_3}{100}[\text{mm}] = 0.1 + \frac{8}{100} = 0.18$ mm

1 Introduction

In this first assignments, the main focus will be on performing crack analysis using finite element method (FEM) in Abaqus software using two approaches. The first method is to perform a pre-defined crack analysis without separation between two materials, whereas the area around the crack tip will be evaluated to obtain the behavior of the stress field. Hence, J-integral will be calculated based on the stress field using domain integral method to obtain the energy release quantity. The key takeaway from this is to find the stable value of J-integral based on the contour integral surrounding the crack, which will be used as a reference value for the crack initiation value.

The second task is to analyze crack propagation using the cohesive zone method. Hence, some cohesive elements will be defined along the pre-defined crack path with the cohesive parameters with an initial crack opening on the front of the cohesive line. From the task definition, the separation behavior of the cohesive are will be observed, as well as the energy release rate. This can be achieved by plotting the traction-separation curve, which will show the relationship between the traction and separation displacement along the cohesive zone. Another key aspect that will be obtained is to know the force-time response during the crack propagation, so that it can be correlated with the traction-separation curve.

2 Set up of the Model

2.1 Material Properties

Table 1: Flow curve data for Q1 and Q2

Plastic Stress (MPa)	Strain
300	0
400	0.001
600	0.003
700	0.005
Young Modulus (GPa)	ν
210	0.3

Table 2: Cohesive parameters for Q2

Material Parameters	Values
K_n (GPa)	210
K_s (GPa)	210
K_t (GPa)	210
σ_n (MPa)	500
$\sigma_{s,t}$	0
δ_{fail} (mm)	0.0038

Table 1 shows the material properties for the elastic and plastic part, which includes the plastic flow with its strain as well as the young modulus and Poisson's ratio for the elastic part. Here, the material will be used for both question 1 and question 2. Meanwhile, table 2 shows the cohesive parameters, which will be used to define the cohesive zone model in question 2. The parameters include the stiffness of the cohesive area in normal and shear directions, the maximum nominal stress, and the failure separation displacement.

2.2 Geometry and Boundary Conditions

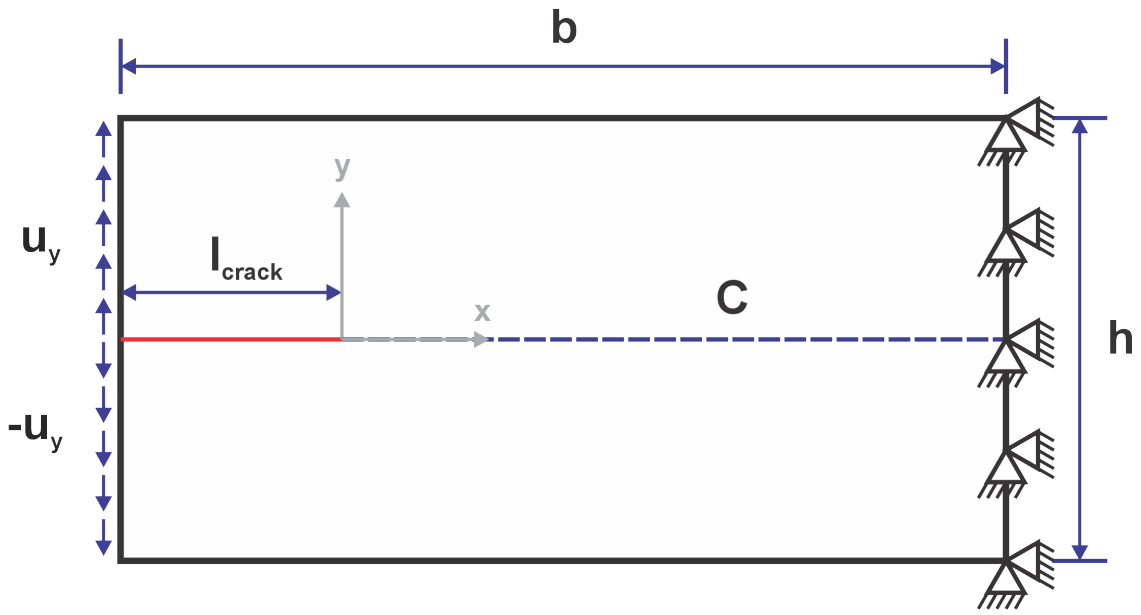

Figure 1: Geometry and boundary definition of the plate with horizontal crack on the left-middle side of the plate. The geometry parameters are defined in the first section of the report, whereas b = 2.4 mm, h = 1.536 mm, and l = 0.504 mm.

Figure 1 shows the geometry and boundary conditions of the plate with horizontal crack. Hence, the displacement will be applied on the left side of the plate, whereas the left-top edge will have displacement to the y-positive direction and left-bottom edge will have the opposite direction. The right side of the plate will be fixed in both x and y directions. The crack is designated as in the red color with some certain length.

2.3 Mesh Set Up

Results and Discussion

Q1: Mesh Sensitivity Analysis of plate with circular hole

... Create the model as shown in figure 1, using the face partitioning illustrated in figure 2, and apply the following assumptions: small deformations, plane stress conditions, and a homogeneous, isotropic, linear elastic material. For each mesh size specified in table 1, create a separate Job. Apply the local mesh size around the hole and use the global mesh size for the remaining regions of the plate.

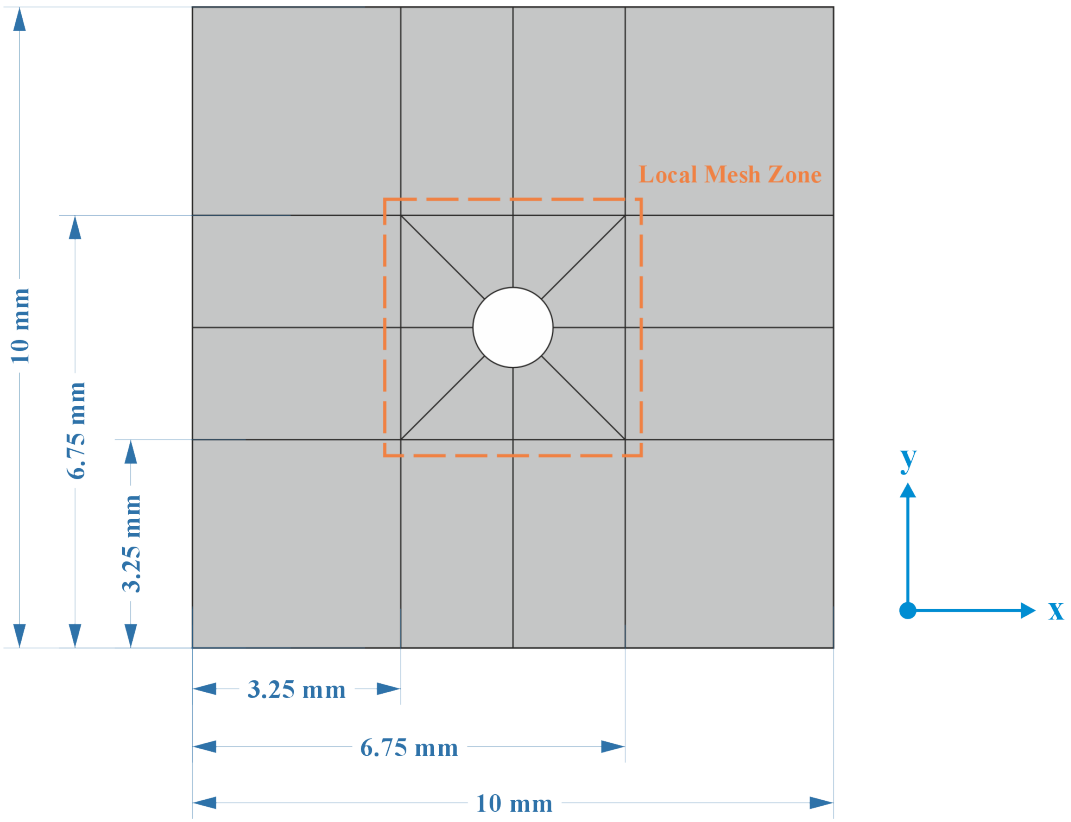

Figure 2: Partitioning guideline in order to create a structured mesh for the plate with circular hole. The whole mesh variations use CPS4, which is a 4-node bilinear plane stress quadrilateral element, also using quad-structured mesh control feature for the whole region to retain structured mesh and avoid extreme-distorted element.

The baseplate with circular hole is mesh using a structured mesh, hence the partitioning is well-defined to ensure a good mesh quality. As requested by the task, the baseplate is partitioned using the general formatting guidelines. However, the author have the freedom to adjust the partitioned size. Therefore, for this assignment the dimensioning of the mesh partition follows the provided Figure 2.

After the plate partitioning, specifically for task 1, the baseplate will be mesh using 8 variations in the mesh size, where it is based on the global and local mesh size. The global mesh size is defined as the mesh size for the entire plate, while the local mesh size is defined as the mesh size around the circular hole (hence is the area inside the small square partition). This method is done in order to capture the stress concentration effects on the area near the hole accurately while maintaining a low computational effort since the mesh size is not fine for the whole plate.

In order to know the mesh influence on the results, a mesh sensitivity analysis is performed. This analysis involves systematically varying the mesh sizes and observing the effects on the simulation results, particularly the stress distribution around the circular hole. Therefore, mesh variation in table 3 is used for this study, with a different global and local mesh size.

Table 3: Mesh size variations used for mesh sensitivity analysis.

Mesh Number	Global Mesh Size (mm)	Local Mesh Size (mm)
1	1	1
2	1	0.6
3	0.8	0.4
4	0.6	0.3
5	0.4	0.2
6	0.3	0.1
7	0.2	0.05
8	0.1	0.02

Table Description: This table summarizes the eight mesh configurations used in the mesh sensitivity analysis. Each mesh is defined by its global mesh size (applied to the entire plate) and a finer local mesh size (applied around the circular hole) to accurately capture stress concentrations while optimizing computational efficiency.

... For each mesh size, provide a figure exported directly from the Abaqus software (not a screenshot of the interface).

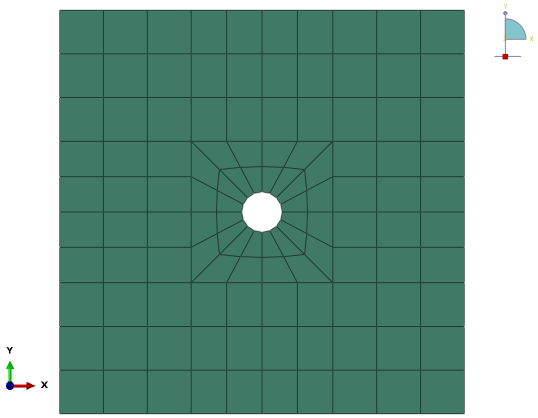

Mesh 1: 116 elements.

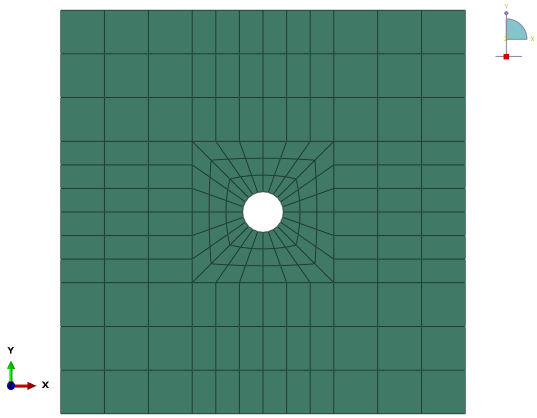

Mesh 2: 180 elements.

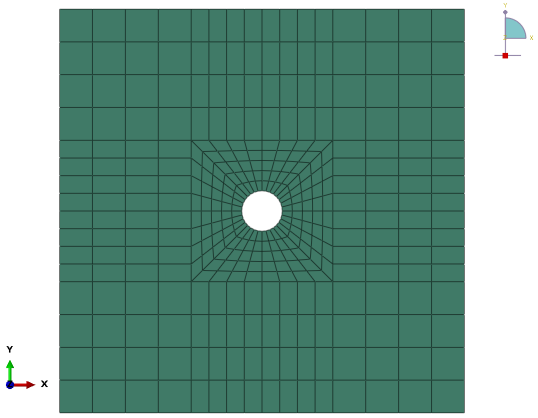

Mesh 3: 352 elements.

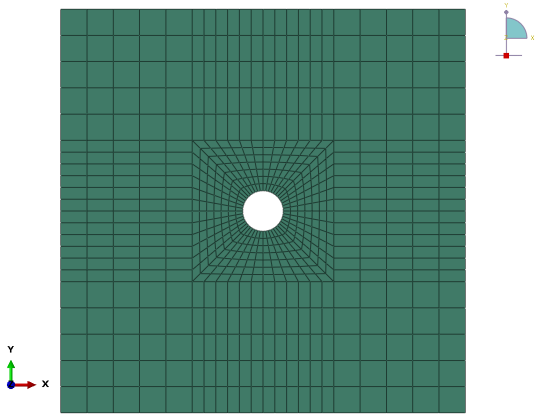

Mesh 4: 676 elements.

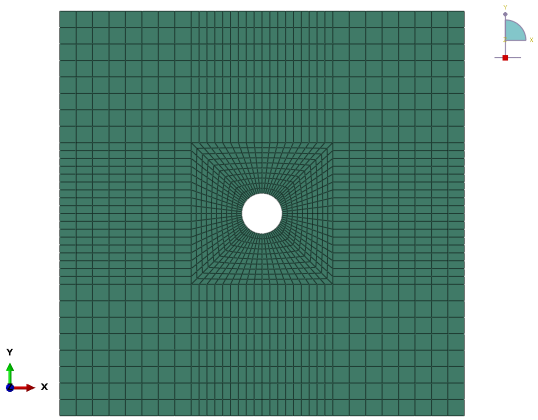

Mesh 5: 1552 elements.

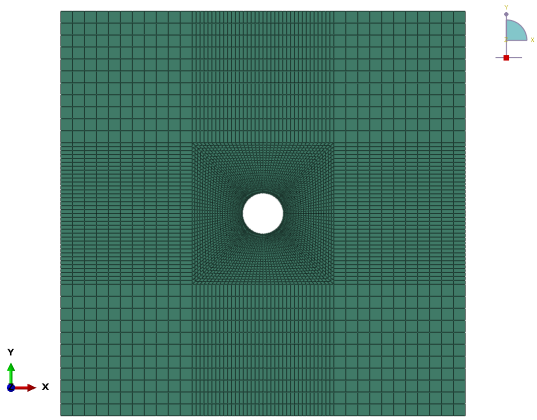

Mesh 6: 4948 elements.

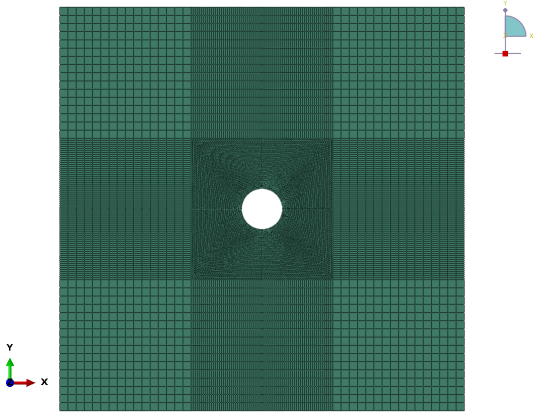

Mesh 7: 16424 elements.

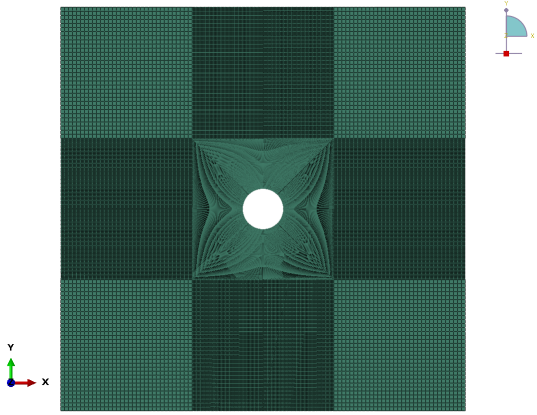

Mesh 8: 97042 elements.

... For each mesh size, provide a contour plot of the relevant stress component, with indicating the locations of both maximum and minimum stress values on the plot. Please ensure the contour plots are clearly presented, and the values are readable.

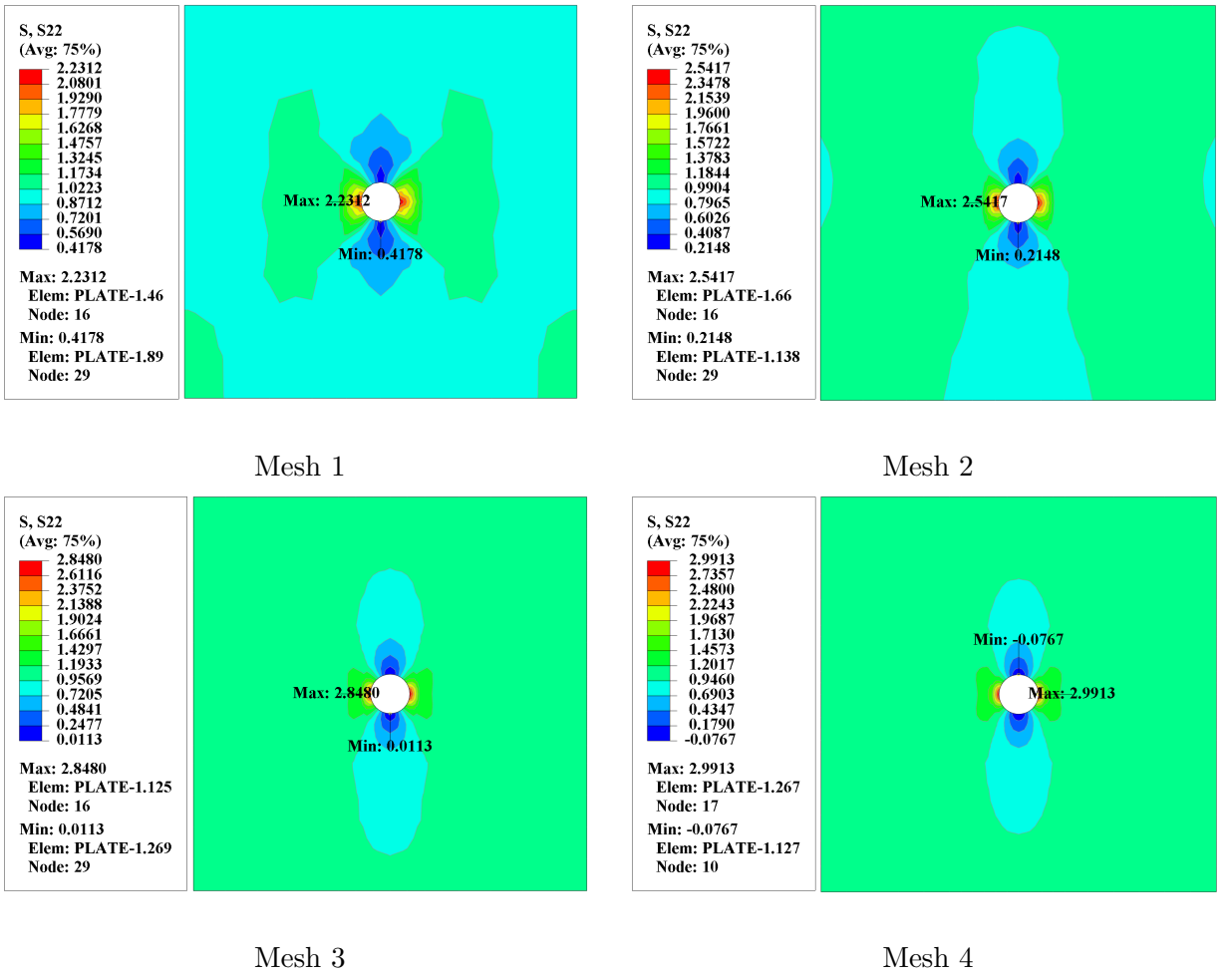

Figure 3: Contour plots of the S_{22} stress component for Mesh 1, 2, 3, and 4 (from left to right, top to bottom). Maximum and minimum stress locations are indicated.

The relevant stress component for this analysis is the S_{22} stress component, which corresponds to the vertical stress in the y-direction. This component is particularly important for this case because the applied load is a uniaxial tensile stress in the vertical direction. Figure 3 shows the contour plots of the S_{22} stress component for the first four mesh sizes. A coarse stress distribution is shown in Mesh 1, with a maximum stress of 2.231 MPa. As the mesh is refined, the maximum area (hence refer to the red area) becomes more localized around the hole, indicating a more accurate capture of the stress concentration effect.

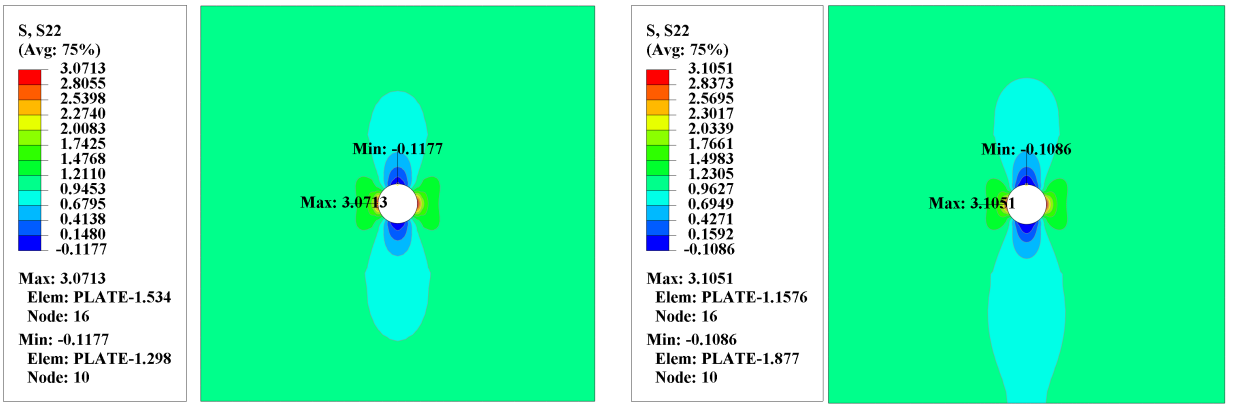

Mesh 5 Mesh 6

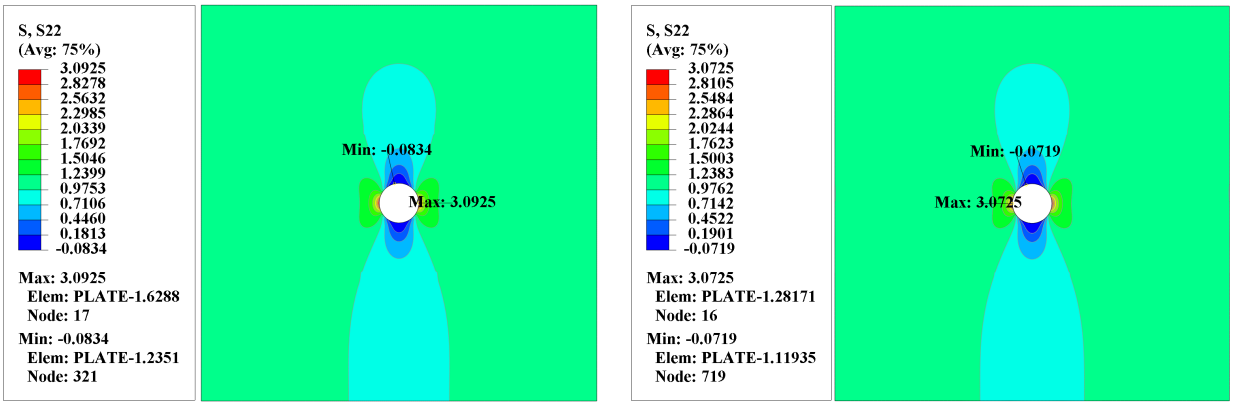

Mesh 7 Mesh 8

Figure 4: Contour plots of the S_{22} stress component for Mesh 5, 6, 7, and 8 (from left to right, top to bottom). Maximum and minimum stress locations are indicated.

As the mesh variation increase up to 1000 elements starting from Mesh 5 variation, the stress distribution becomes more refined. However, there are some enlargement of positive stress below the hole as the mesh is getting finer. This phenomenon can occur due to the interaction between the mesh refinement and the stress gradient around the hole.

... For each mesh size, calculate the stress concentration factor $K_t = \sigma_{max}/\sigma_{nom}$, You are required to provide two plots: the first plot should show eight curves (one for each mesh size), the relevant stress over the path. The second plot should display the mesh number against K_t. Based on the results, discuss and justify which mesh provides the most accurate and efficient representation of stress concentration, and explain why it should be chosen.

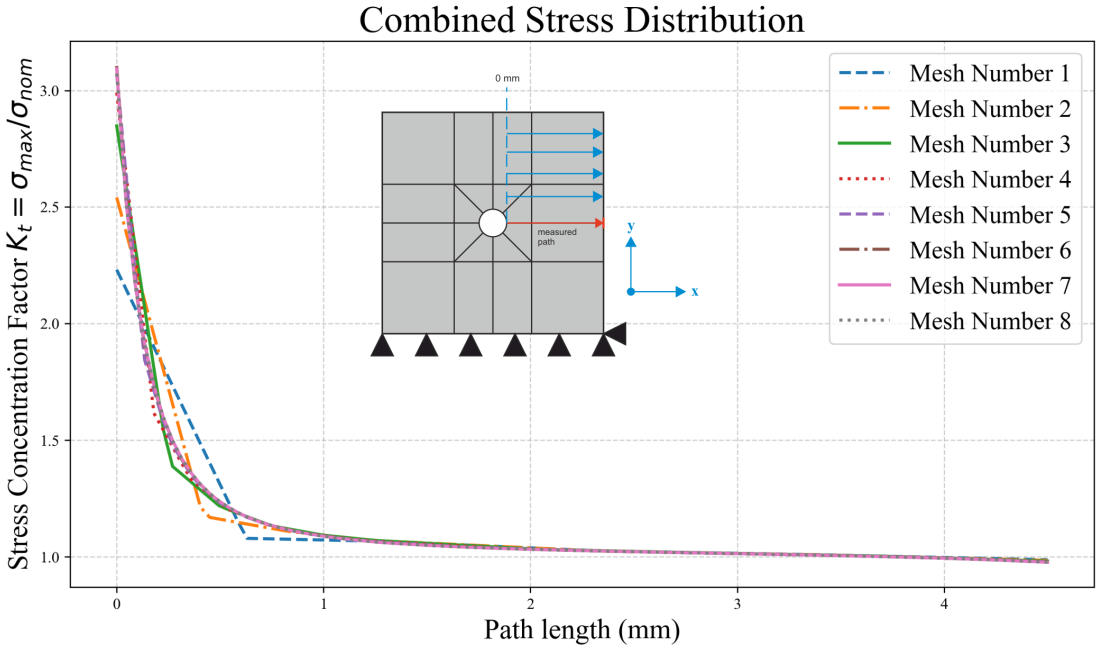

Figure 5: Stress concentration distribution along the defined path for all mesh sizes. Each curve represents the relevant stress component for a specific mesh configuration, illustrating the effect of mesh refinement on capturing the stress concentration near the circular hole. The path is defined from the edge of the hole to the opposite edge of the plate, marked by redline in the geometry. The stress concentration factor is calculated based on the ratio of generated stress or maximum stress in the specific point to the nominal stress, which is 1 MPa.

Figure 5 shows the stress distribution of the S_{22} stress component along the defined path for all mesh sizes. As the mesh is refined, there are some tendencies that appear in the development of the stress distribution curve. The first tendency is the maximum stress value is increasing as the mesh is getting finer. This is due to the fact that a finer mesh can capture the stress concentration more accurately, leading to higher peak stress values. However, after Mesh 6 variation, the maximum stress value starts to decrease slightly as shown in figure 6. This indicates that the solution is converging, and further mesh refinement does not significantly change the results.

The second tendency is the overall shape of the stress distribution curve becomes smoother as the element size decreases. This is because a finer mesh has the ability to capture the stress gradients more accurately, resulting in a more continuous stress curves along the path.

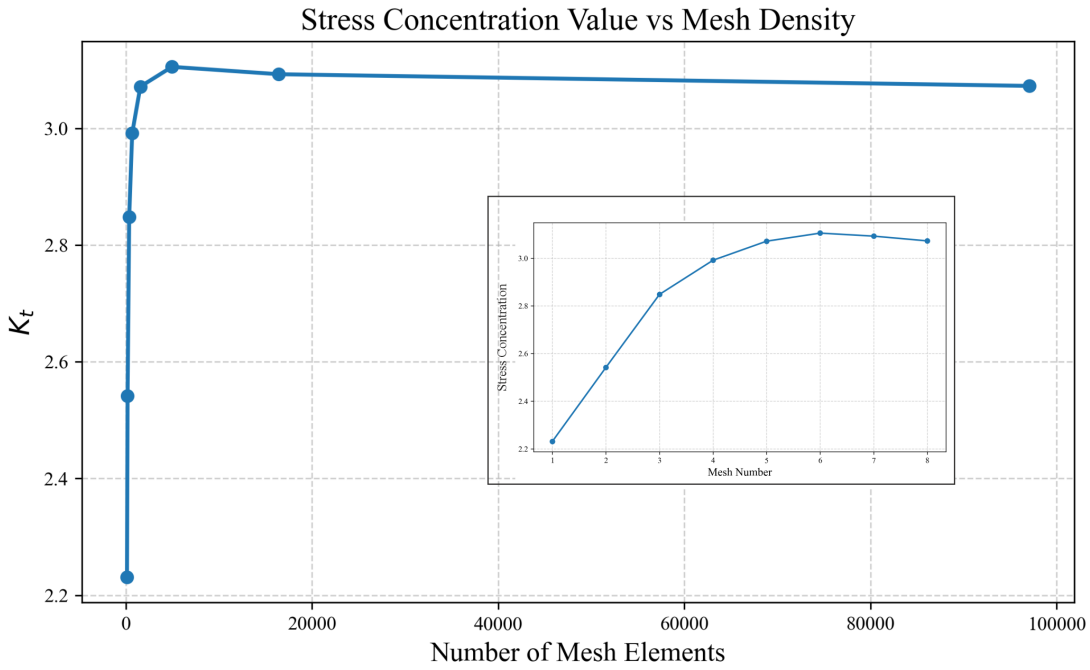

Figure 6: Stress concentration factor K_t along the defined path for all mesh sizes. Each curve represents the K_t value for a specific mesh configuration, illustrating the effect of mesh refinement on capturing the stress concentration near the circular hole. The plot is divided by two plots, where the main plot shows the overall K_t value based on the element numbers that being used, while the zoomed-in plot shows the detail of K_t value based on specifically the mesh numbering.

Based on these results, mesh number 3 is chosen as the most optimal mesh sizing configuration. As we refer to the classical value of K_t, which is $K_t \approx 2.72$ for plate structures with ratio of 0.1 based on Figure7 from the appendix of the assignment 2, as we see that mesh 3 provides a K_t value that is in close agreement with this classical solution. This indicates that the mesh is sufficiently refined to capture the stress concentration effects accurately without being overly computationally expensive. It is possible that to use more refined mesh than mesh 8, since the curve is about to converge to value of 2.72. However, the computational cost will become significantly higher, while the improvement in accuracy will not be substantial. Therefore, mesh 3 is selected as the optimal mesh for this analysis, balancing accuracy and efficiency.

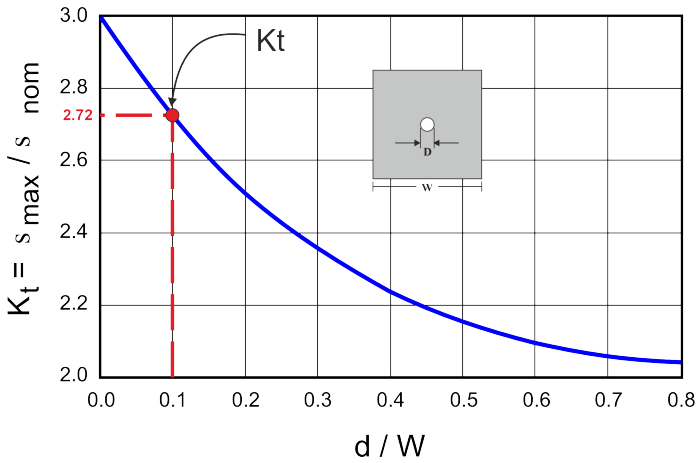

Figure 7: Plot of the stress concentration factor K_t versus mesh number for all mesh configurations. For this case, it shows that the effective K_t for d/W = 0.1 is approximately 2.72. Hence, this will be a reference to choose the most optimal mesh size configuration.

... Taking advantage of the symmetry in both the geometry and the boundary conditions, propose a simplified model that reduces computational cost and simulation time. Create and submit two figures: one showing the mesh of the proposed model, and the other displaying contour plot of the relevant stress distribution. Compare it to the original model.

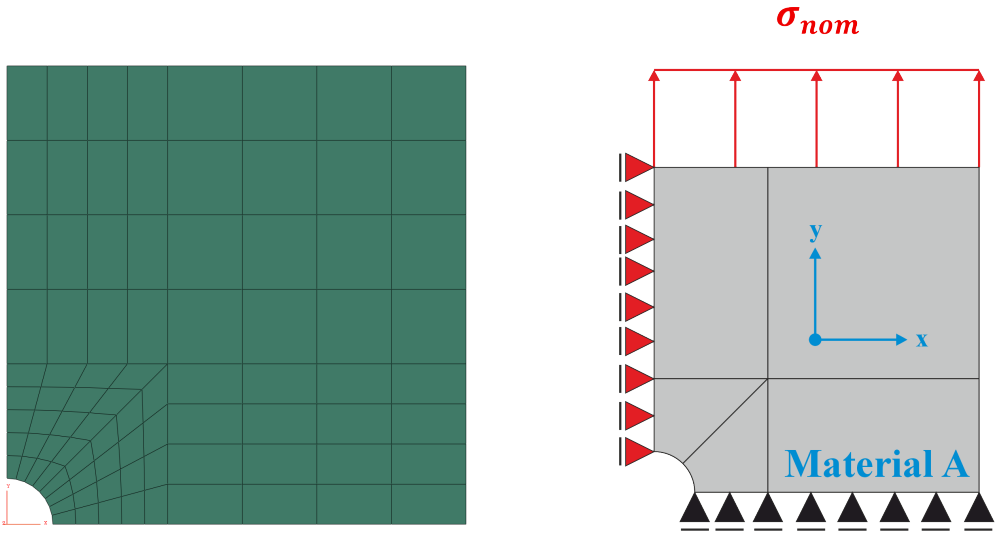

Figure 8: (Left) Mesh of the proposed quad-symmetry model. (Right) boundary conditions configuration applied to the half model. Additional boundary condition is applied to the symmetry line, which here restrict the horizontal movement while allowing y-axis movement. The restriction on the right bottom corner is omitted since it is already restricted by the symmetry line for the horizontal movement. The nominal stress is applied on the top line as in the full model, as well for the fixed support on the bottom that allows horizontal movement.

The symmetry is modeled as in figure 8, where the mesh is created using the same mesh size as in Mesh 4 variation. Modification of boundary condition is done as in figure 8 so that the symmetry model can represent the full model. After running the simulation, the stress contour plot is shown in figure 9. It can be seen that the stress distribution for the symmetry model is almost identical with the full model. The value of maximum stress and minimum stress is also the same for both cases. There are some slightly deviation in both maximum and minimum S_{22} stress values. Hence by utilizing symmetry, the computational cost and simulation time can be significantly reduced by calculating fewer areas which represent the full model.

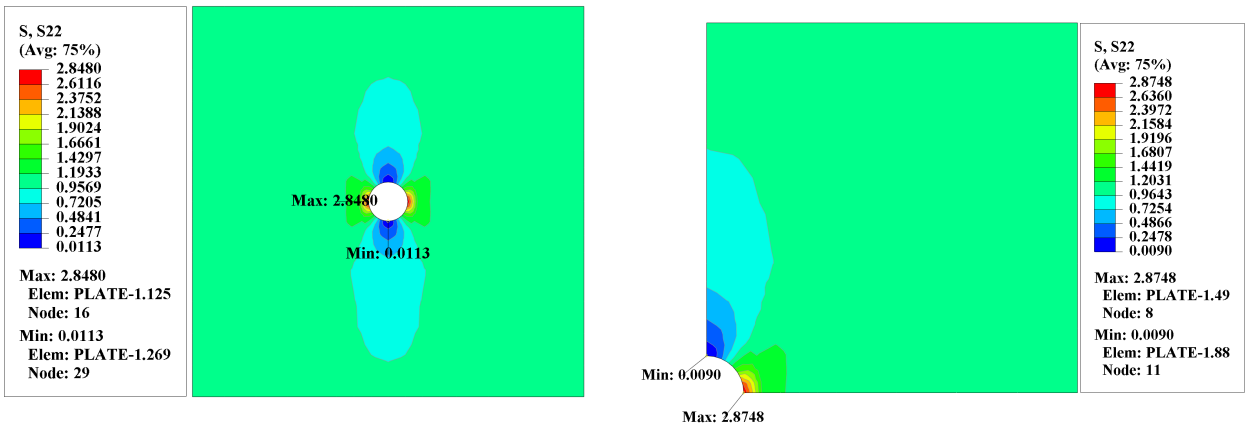

Full model

Quad-symmetry model

Figure 9: Comparison of S_{22} stress contours for Mesh 3: full model (left) and quad-symmetry model (right). Both plots show the stress distribution and concentration near the hole, demonstrating that the quad-symmetry model accurately reproduces the results of the full model, with slighly deviation on the values.

Q2: Investigate the effects of isotropic and kinematic hardening on the mechanical behavior of a material

In this question, the focus will be to investigate the isotropic and kinematic hardening effect to its mechanical response. The analysis will be conducted using an uniaxial tensile test model, where the geometry is from previous question 1. But here instead of using a nominal stress $\sigma_{nominal}$, a displacement of 0.2 mm will be applied to the top edge of the plate, while the rest of the boundary conditions is similar as in figure 2. However, since hardening effects would be investigated, cyclic loading will be applied to the model. A cyclic amplitude in figure 10 is used to perform the cyclic loading simulation based on the total displacement of 0.2 mm.

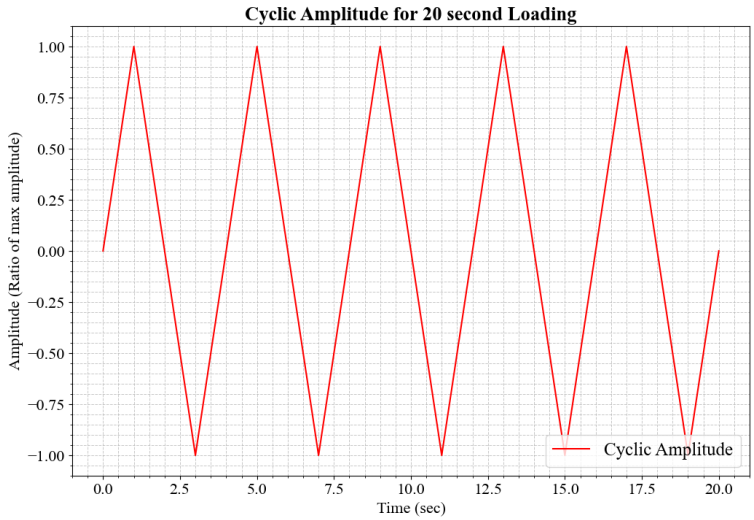

Figure 10: Applied cyclic loading amplitude for the tension-compression simulation. The plot shows the displacement history used to investigate the hardening behavior under repeated loading cycles. The amplitude is defined to reach a maximum displacement of 0.2 mm as the peak value is reached, while the minimum displacement is set to -0.2 mm when the valley is reached. This loading pattern is applied for 5 cycles and the total time duration of 20 seconds.

... ***Isotropic Hardening Model:*** *Set the material parameters for the isotropic hardening model, keeping kinematic hardening deactivated. Perform a cyclic loading simulation (tension-compression) using the amplitude plotted in figure 3. Plot and analyze the stress-strain hysteresis loops.*

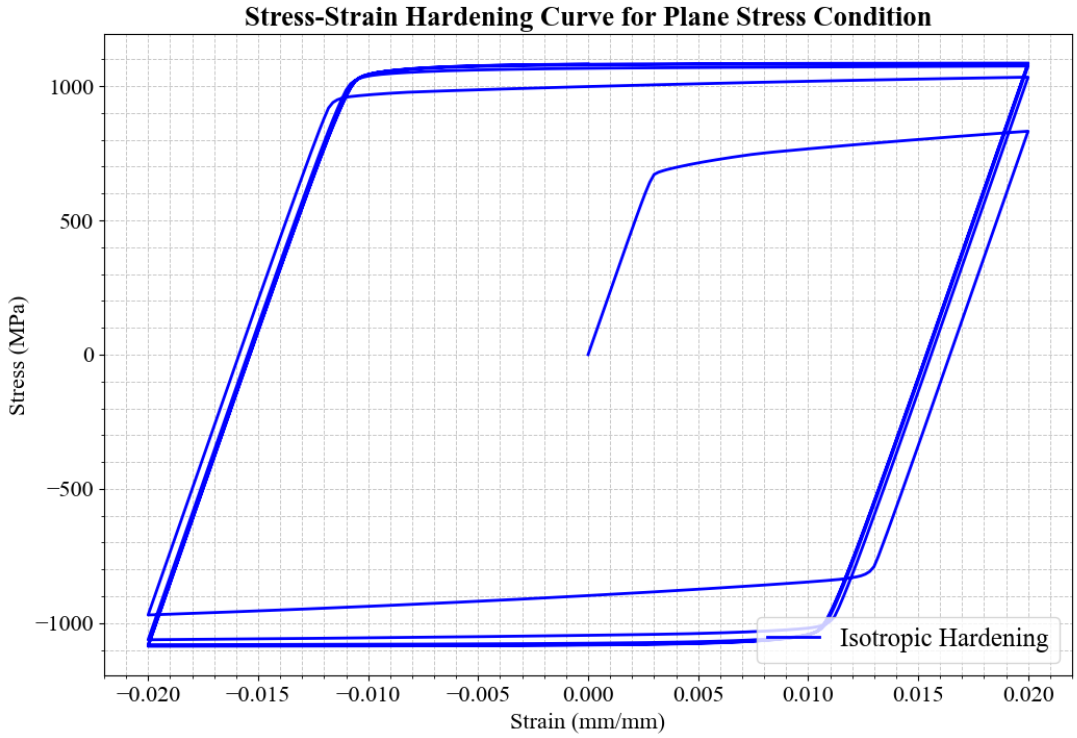

Figure 11: Stress-strain hysteresis loop for the isotropic hardening model under cyclic tension-compression loading. The plot illustrates the expansion of the yield surface and the corresponding material response. For this isotropic hardening model, Q-infinity and hardening parameter b are set according to table **??**, whereas the C_1, γ_1, and C_2 are set to zero to disable the kinematic hardening effect.

Figure 11 shows the stress-strain hysteresis loop for the isotropic hardening model under cyclic tension-compression loading. As the cyclic load applied, at first cycle the material starts to yield at the initial yield stress of 732 MPa. As the loading continues and changing direction to compression, the yield surface starts to expand isotropically, leading to an increase in the yield stress for subsequent cycles. This expansion of the yield surface is characteristic of isotropic hardening, where the material's resistance to plastic deformation increases uniformly in all directions.

... ***Kinematic Hardening Model:*** *Set the material parameters for the kinematic hardening model, assuming no isotropic hardening. Perform a cyclic loading simulation (tension-compression) using the amplitude plotted in figure 3. Plot and analyze the stress-strain hysteresis loops.*

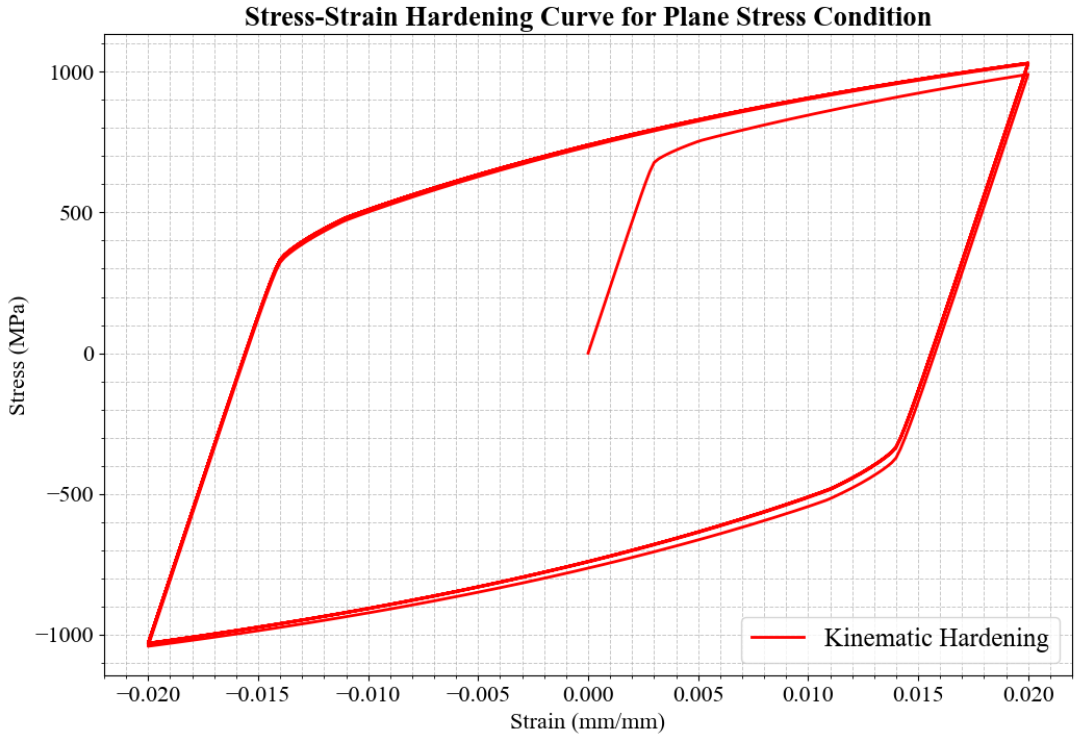

Figure 12: Stress-strain hysteresis loop for the kinematic hardening model under cyclic tension-compression loading. The plot demonstrates the translation of the yield surface and the corresponding material response. For this kinematic hardening model, Q-infinity and hardening parameter b are set to zero to disable the isotropic hardening. While parameters such as C_1, γ_1, and C_2 are set according to table **??** in order to activate kinematic hardening.

Figure 12 shows the stress-strain hysteresis loop for the kinematic hardening model under cyclic tension-compression loading. Unlike the isotropic hardening case, the yield surface translates in the stress space without changing its size. This behavior indicates that kinematic hardening occurs, where the material's yield surface moves in response to plastic deformation, allowing for a more accurate representation of the Bauschinger effect.

... Compare the extracted curves from previous questions and discuss the results.

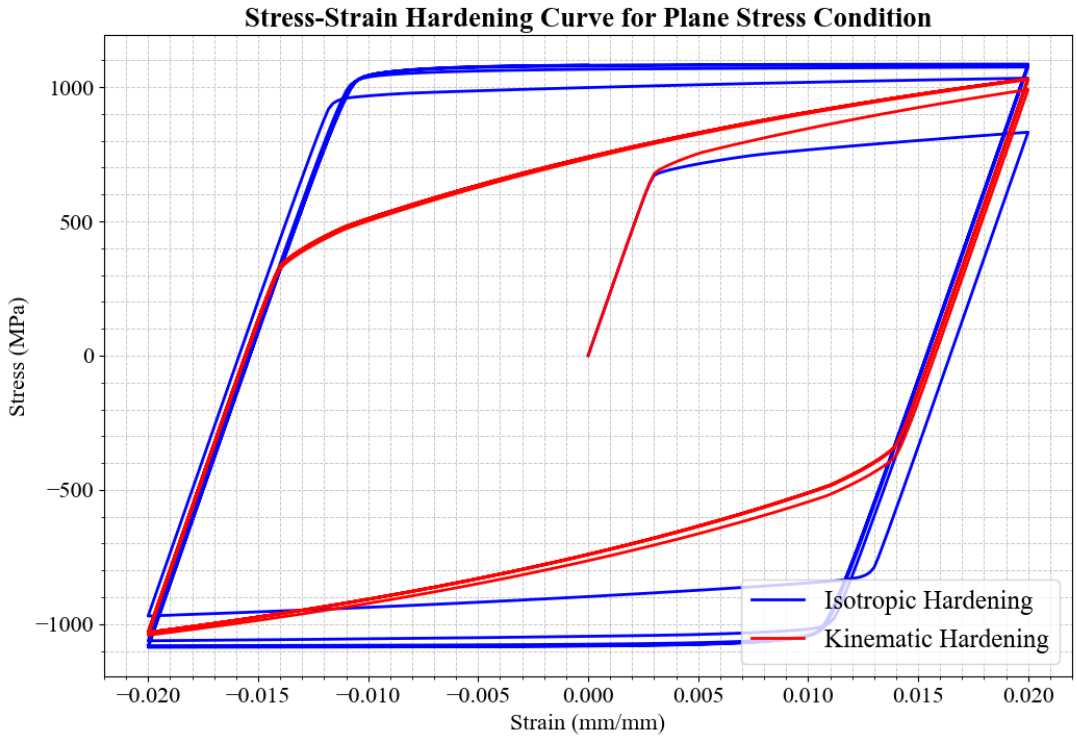

Figure 13: Comparison of stress-strain hysteresis loops for isotropic and kinematic hardening models under cyclic tension-compression loading. The plot highlights the differences in material response due to both hardening mechanisms.

Figure 13 shows the comparison of stress-strain hysteresis loops for isotropic and kinematic hardening models under cyclic tension-compression loading. The isotropic hardening model exhibits a symmetric hysteresis loop, indicating uniform expansion of the yield surface in all directions. In contrast, the kinematic hardening model shows an asymmetric hysteresis loop, reflecting the translation of the yield surface in response to plastic deformation. The difference from these two models is obvious, where the isotropic hardening model shows a larger area within the hysteresis loop, indicating higher energy dissipation during cyclic loading. This is due to the uniform increase in yield stress that allows in this model. While in the kinematic hardening model, increase in yield stress does not occur, only shifting of yield surface is allowed. Hence, the energy dissipation is lower compared to the isotropic hardening model.

... Simulate the model using combined hardening law parameters in table 2. Compare the results with those obtained using isotropic and kinematic hardening parameters. Discuss how variations in the combined hardening parameters influence the material behavior.

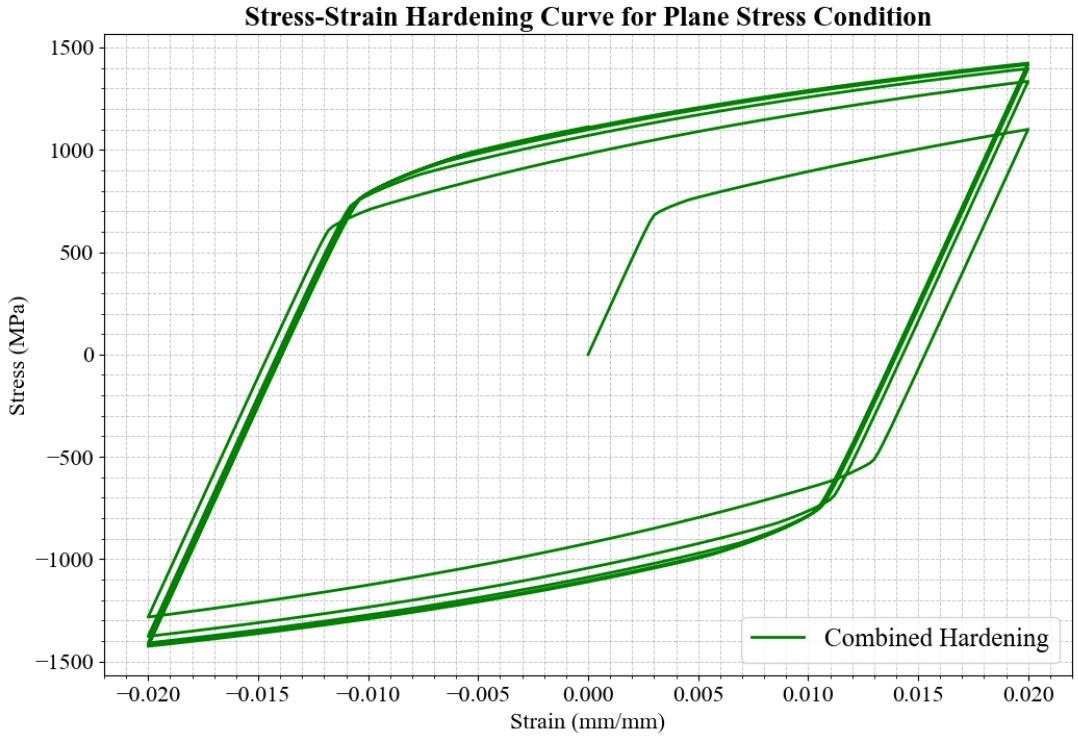

Figure 14: Stress-strain hysteresis loop for the combined hardening model under cyclic tension-compression loading. The plot shows the material response when both isotropic and kinematic hardening mechanisms are active, illustrating the combined effects on the expansion and translation of the yield surface.

As both of the model are combined, the stress-strain hysteresis loop for the combined hardening model is shown in figure 14. This shows a unique material behavior, whereas the cyclic loading is applied, the yield surface expands isotropically as well as translating in the stress space. This combined effect results in a more complex hysteresis loop, which reflects the play role between isotropic and kinematic hardening mechanisms. The combined hardening model produced a larger hysteresis loop area compared to the kinematic, as well as for the isotropic hardening model.

This is because the combined hardening model incorporates both of the hardening model, so that it have the ability to increase the yield stress surface as well shifting the yield surface. Therefore, the energy dissipation during cyclic loading is higher than the other two models by looking at the hysteresis loop area. A comparison of all three hardening models is shown in figure 15.

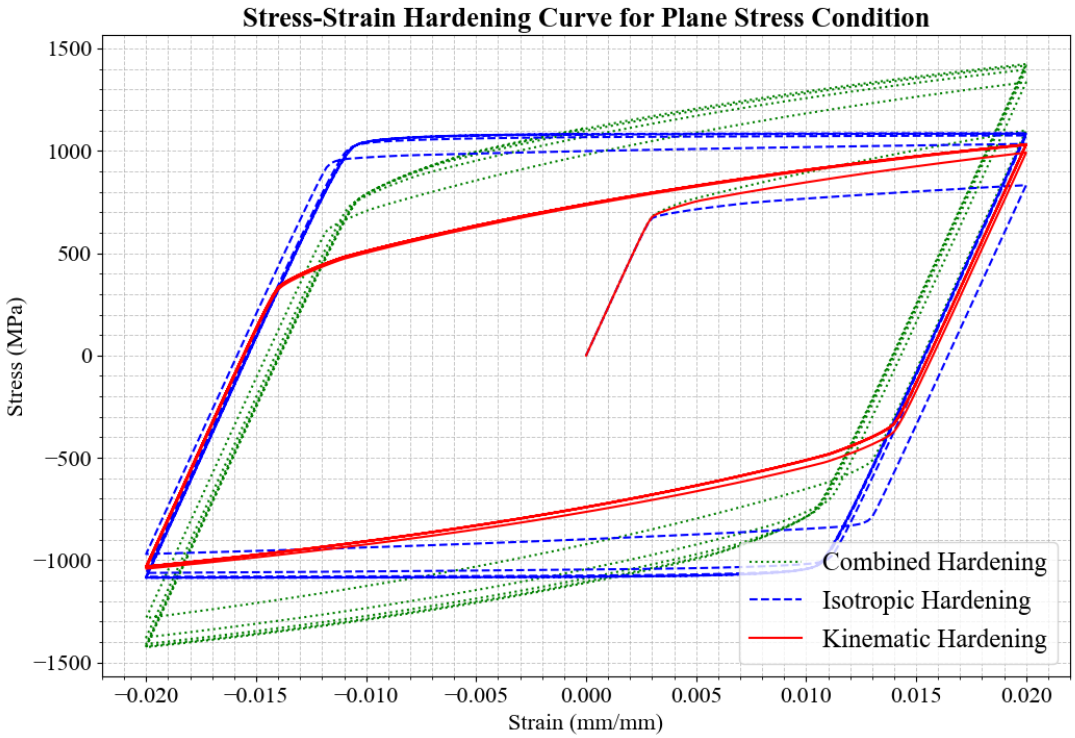

Figure 15: Comparison of stress-strain hysteresis loops for isotropic, kinematic, and combined hardening models under cyclic tension-compression loading. The plot highlights the differences in material response due to these three hardening mechanisms. It shows that when the first time material yielded, both 3 hardening mechanism are having the same transitional elastic-plastic breaking point. However, as the loading increase, combined hardening have the highest hardening modulus, where this is shown by the highest hardening development (steeper slope) compared to the kinematic and isotropic hardening model.

Q3: Standard and UMAT subroutine for J2 plasticity

... Read the provided J2 UMAT, then decide to choose plane stress or plane strain condition, add a screenshot that shows the code lines where this choice is made and where elastic stiffness and equivalent von mises stress is calculated, and give an explanation based on the lecture.

```
1  C ------------------------------------------------------------------
2  C UMAT FOR ISOTROPIC ELASTICITY AND ISOTROPIC MISES PLASTICITY
3  C CANNOT BE USED FOR PLANE STRESS
4  C
5  C PROPS(1) - E
6  C PROPS(2) - NU
7  C PROPS(3...) - YIELD AND HARDENING DATA
8  C CALLS UHARD FOR CURVE OF YIELD STRESS VS. PLASTIC STRAIN
9  C ------------------------------------------------------------------
```

Code section in the UMAT where the plane strain or plane stress condition is selected. This determines the appropriate constitutive behavior for the simulation. Hence, it is stated explicitly in the header 2nd and 3rd line that this UMAT subroutine cannot be used for plane stress condition.

```
10 C      ELASTIC STIFFNESS
11 C
12       DO K1=1, NDI
13         DO K2=1, NDI
14           DDSDDE(K2, K1)=ELAM
15         END DO
16         DDSDDE(K1, K1)=(EG2+ELAM)
17       END DO
18         DDSDDE(K1, K1)=EG
19       END DO
```

Code lines in the UMAT where the elastic stiffness matrix is calculated. This matrix defines the linear elastic response of the material.

```
20 C CALCULATE EQUIVALENT VON MISES STRESS
21 C
22       SMISES=(STRESS(1)-STRESS(2))**2+(STRESS(2)-STRESS(3))**2
23      1          +(STRESS(3)-STRESS(1))**2
24       DO K1=NDI+1,NTENS
25         SMISES=SMISES+SIX*STRESS(K1)**2
26       END DO
27       SMISES=SQRT(SMISES/TWO)
```

This code section in the UMAT where the equivalent von Mises stress is computed. This value is used to evaluate yielding according to the J2 plasticity criterion. From these three snippets shows the code section of the UMAT subroutine file in which explicitly stated that the simulation should use plane strain instead of plane stress. This is done by set up the mesh type that will be used in the simulation, whereas plane strain mesh type, hence CPE4 (A 4-node bilinear plane strain quadrilateral) in Abaqus, is utilized. Another supporting facts that this model is using plane strain condition is stated in the equation definition of the elastic stiffness matrix in the second snippets, as well for Von Misses stress calculation in third snippets. Where in both equations, the UMAT subroutine file is considering the out-of-plane stress component, σ_{33}, which for other case is zero in plane stress condition. From the lecture, σ_{33} have the relation as follows:

$$\sigma_{33} = \nu(\sigma_{11} + \sigma_{22}) = \frac{E\nu}{(1+\nu)(1-2\nu)}(\varepsilon_{11} + \varepsilon_{22}) \tag{2}$$

Whereas in this equation, σ_{33} is expressed using the in-plane stress components (which here is the 11 and 22 component) and the material properties such as Young's modulus, E, and Poisson's ratio, ν.

... Run two simulations with a displacement of 0.5 mm and same material properties: one with the Abaqus embedded J2 model and one with UMAT. Plot, compare, and discuss the true stress-strain curve for both cases.

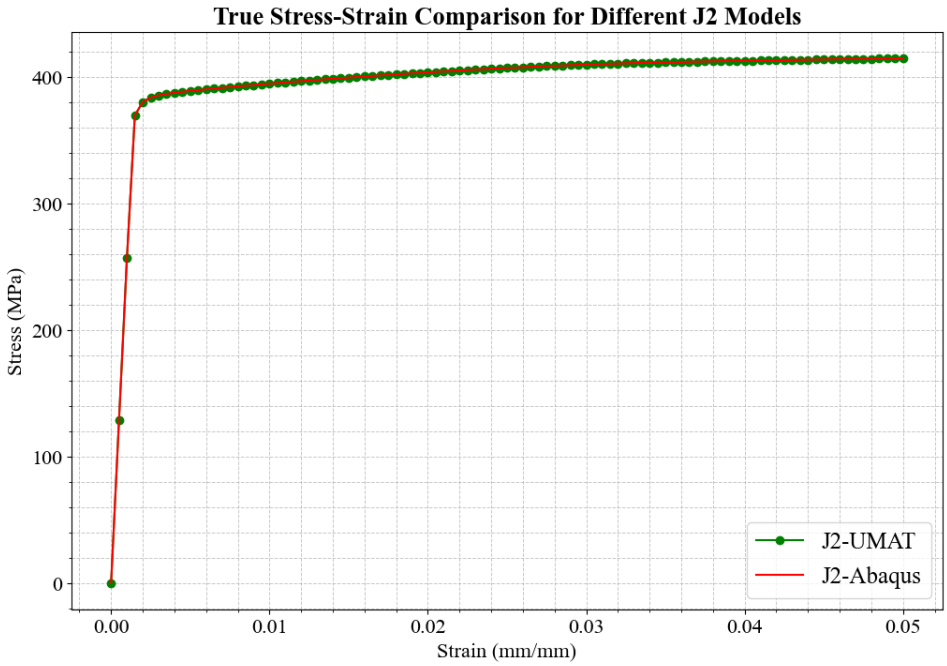

Figure 16: Comparison of tensile test for both J2-UMAT and J2-Abaqus model using the effective mesh variation from Q1. The plot shows the true stress-strain curves for both models, illustrating a linear behavior are shown for both models in the elastic region, followed by a transitional elastic-plastic region in the yielding point at strain about 0.002, and then followed by a plastic region where the curve is none-linear.

Figure above shows the true stress-strain curves for J2-UMAT model and J2-Abaqus. Both of the curve having the same overall behavior in the elastic and plastic area. The elastic-plastic transition and the plastic region seems to have the exact behavior, which hence illustrated using a dot curve that plot for each model, where for each data points both curves showing the exact same results.

... From the embedded J2 simulation, select four representative time frames that trace the evolution from the purely elastic status to the onset of localized necking, present for each frame a contour plot of von Mises stress and equivalent plastic strain. Describe the deformation process of the plate with a hole.

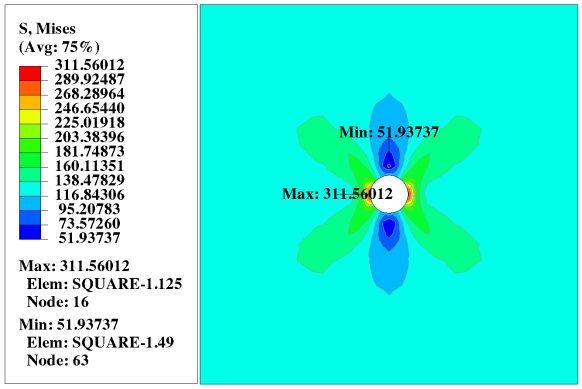

(a) von Mises stress, Frame 1

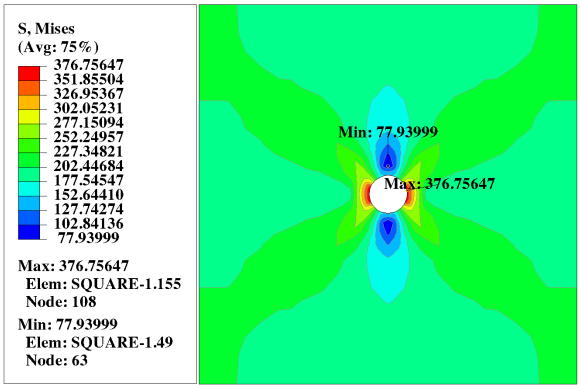

(b) von Mises stress, Frame 2

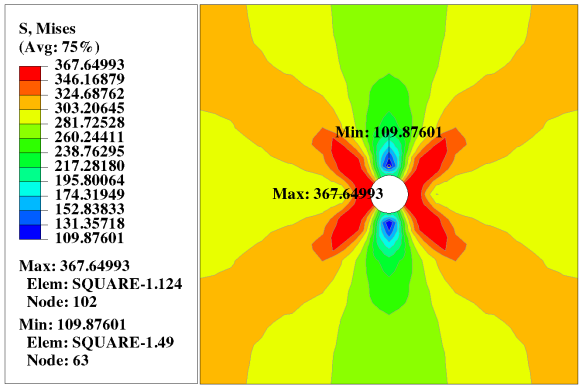

(c) von Mises stress, Frame 3

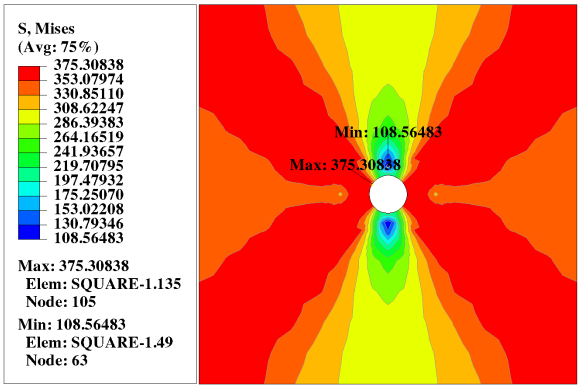

(d) von Mises stress, Frame 4

Figure 17: Contour plots of von Mises stress at four representative time frames from the embedded J2 simulation, showing the evolution from elastic to localized necking. The von Mises stress grows starting from the initial loading phase in time frame 1, where it is at the elastic region. At frame 2, it starts to deform plastically as the stress distribution starts to yield.

Figure above shows the contour plots of the J2-Abaqus model development. The extracted plot starts from frame 1 in figure 17(a), where the material is still in elastic state, with a flower distribution that consist of 6 petals shape-like, whereas the upper and lower petals have the lower stress distribution from 51 to 95 MPa, and the four diagonal petals have stress in range of 138 until 203 MPa. This elastic state also can be shown in figure 18(a),

where the equivalent plastic strain is zero in this state.

As the loading starts to increase, transitional phenomenon occurs in the second frame, shown in figure 17(b). The stress distribution shape starts to change as the petals shape is having the different form and stress value. The red area in the left and right side of the hole start to expand, indicating that the stress concentration starts to propagate. This is also proven in figure 18(b), where the equivalent plastic strain starts to develop as from the left and right side of the hole.

As the loading continues to increase to frame 3 and 4, it is shown from the PEEQ contour in figure 18(c) and (d) that the plastic strain starts to localize in the left and right side of the hole. Then the plastic strain start to grow diagonally to the top-right and left; and bottom-right and left side of the hole. This indicates that the material is undergoing significant plastic deformation in the regions, leading to a localized necking effect.

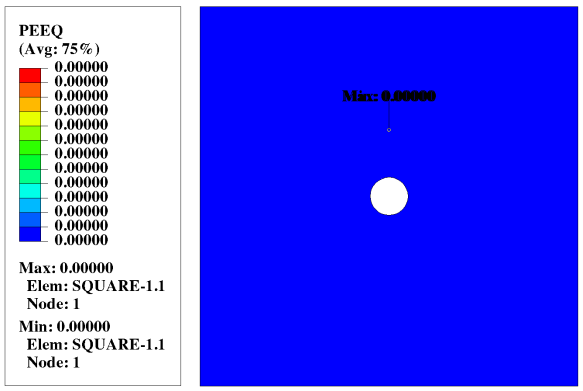

(a) Equivalent plastic strain, Frame 1

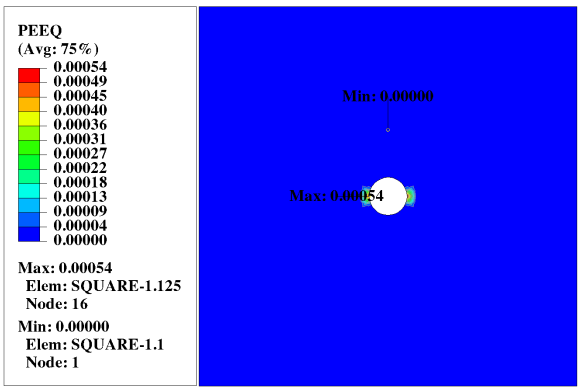

(b) Equivalent plastic strain, Frame 2

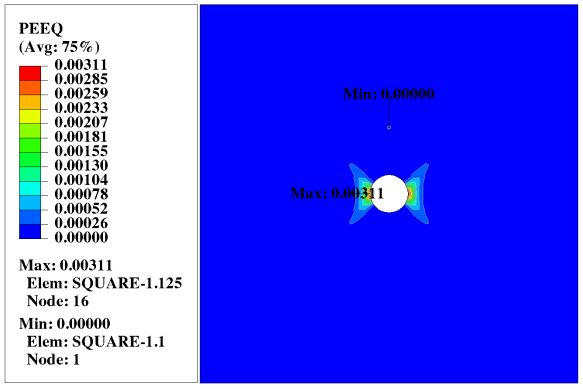

(c) Equivalent plastic strain, Frame 3

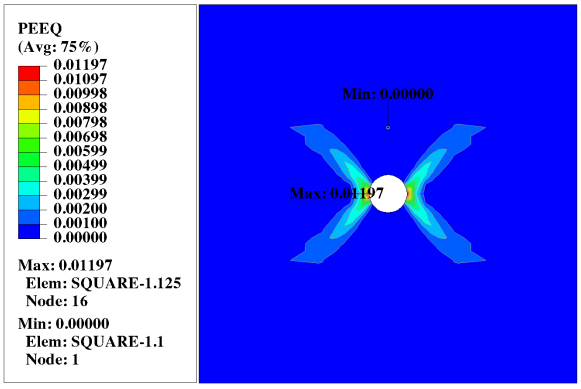

(d) Equivalent plastic strain, Frame 4

Figure 18: Contour plots of equivalent plastic strain at four representative time frames from the embedded J2 simulation, illustrating the progression of plastic deformation and localization.

... From the UMAT simulation, plot the distribution of the relevant stress and plastic strain components for the final time, indicating the meaning of the different SDVs, showing the maximum and minimum location, then discussing the results for different regions.

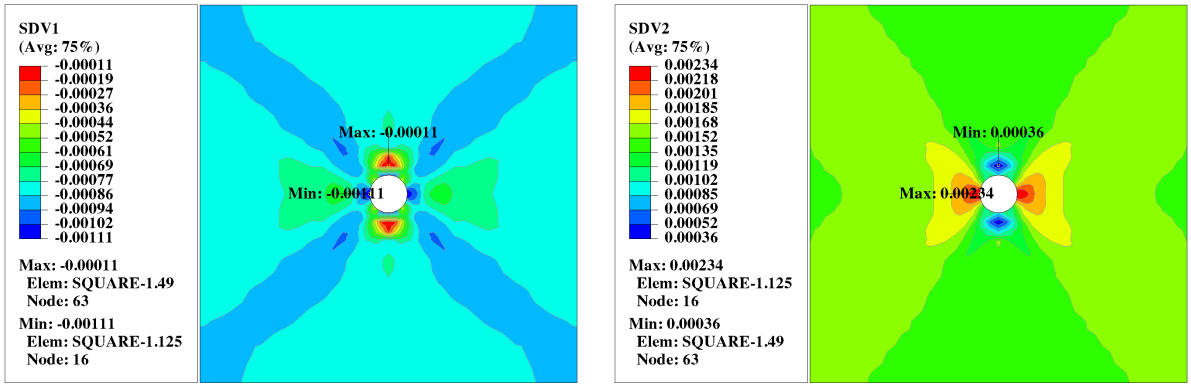

SDV1: ε^e_{11} SDV2: ε^e_{22}

Figure 19: SDV1 and SDV2: Distributions of the first and second state-dependent variables at the final simulation time, showing relevant stress/plastic strain components and internal variables. Maximum and minimum locations are indicated.

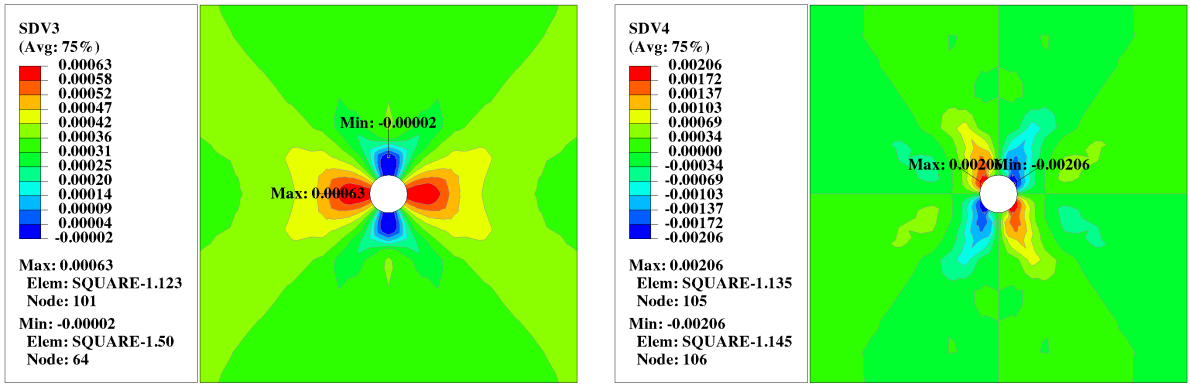

SDV3: ε^e_{33} SDV4: γ^e_{12}

Figure 20: SDV3 and SDV4: Distributions of the third and fourth state-dependent variables at the final simulation time, indicating mechanical quantities and localization effects.

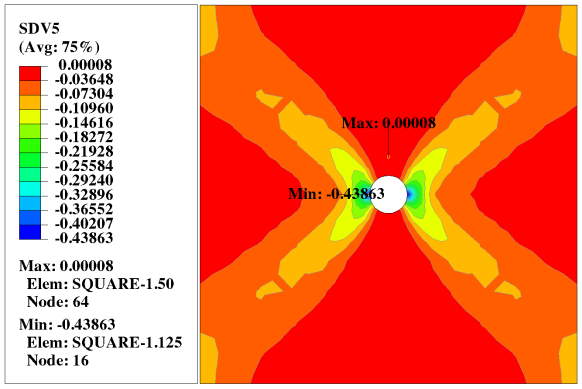

SDV5: ε_{11}^{p}

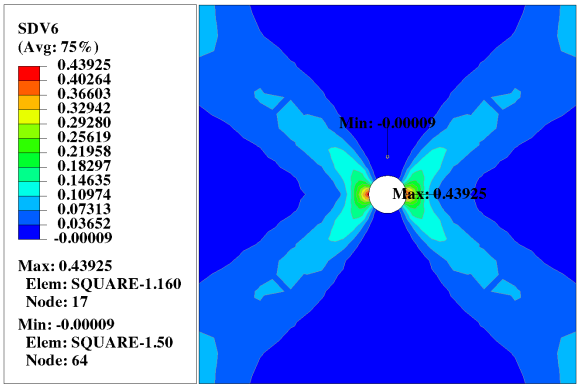

SDV6: ε_{22}^{p}

Figure 21: SDV5 and SDV6: Distributions of the fifth and sixth state-dependent variables at the final simulation time, highlighting regions of maximum/minimum and mechanical response evolution.

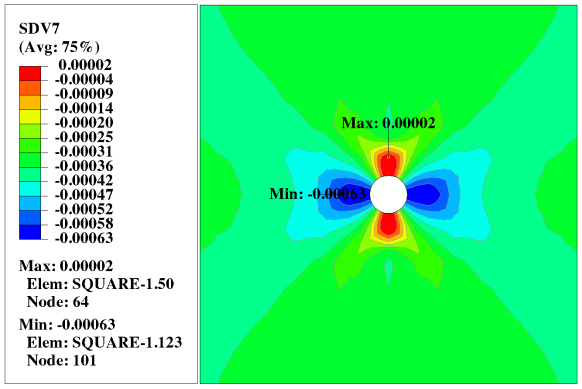

SDV7: ε_{33}^{p}

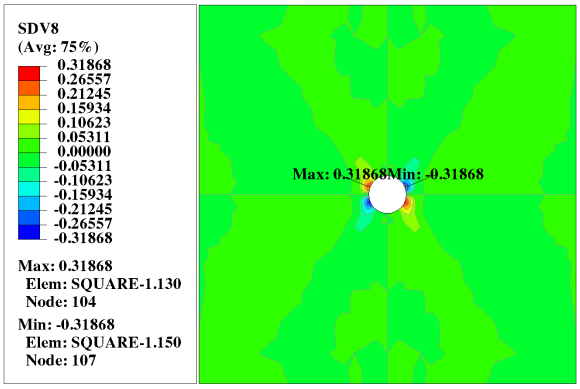

SDV8: γ_{12}^{p}

Figure 22: SDV7 and SDV8: Distributions of the seventh and eighth state-dependent variables at the final simulation time, showing spatial variation and marked extrema.

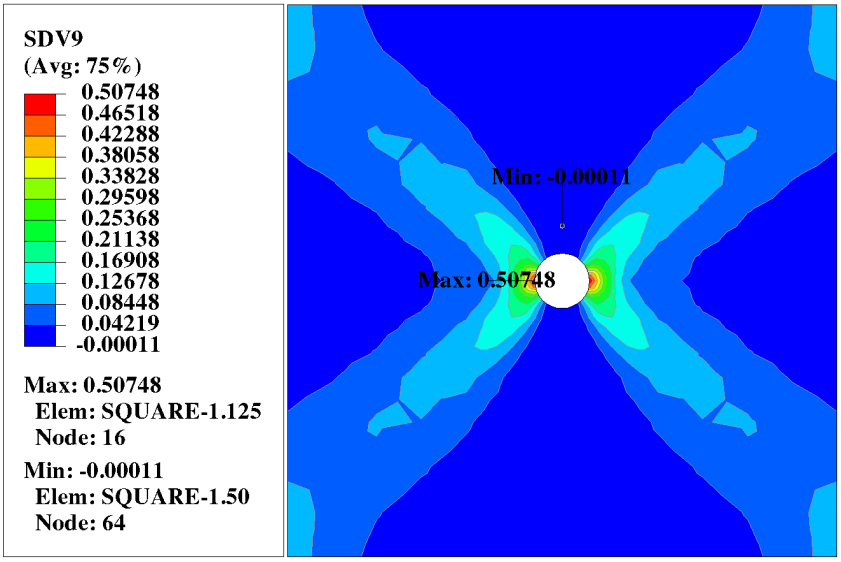

Figure 23: SDV9: Distribution of the ninth state-dependent variable (SDV9): $\bar{\varepsilon}^p$

Figure 19 until figure 23 show the contour plot of all State Dependent Variables (SDVs) at the final simulation time from the J2-UMAT model. For SDV1 until SDV4, these show the parameter components in elastic region, whereas SDV1, SDV2, and SDV3 represent the normal elastic strain components, and SDV4 represents the shear elastic strain component. Then SDV5 until SDV8 show the parameter components in plastic region, where SDV5, SDV6, and SDV7 represent the normal plastic strain components, and SDV8 represents the shear plastic strain component. Finally, SDV9 represents the equivalent plastic strain (PEEQ), which is a scalar measure of the accumulated plastic deformation.

The first observation is that the maximum and minimum values for each SDV are located in different regions of the plate. As SDV1 and SDV5 is compared, The largest elastic and plastic strain for both cases is at compressive state. This can be look, whereas a notch concentration are generated in the left and right side edge of the hole. Hence, the compressive state is caused by the Poisson effect, where the material tends to shrink laterally when stretched along the load direction. Hence, both elastic and plastic distribution show an agreement, showing the dominated compressive state in the same region, despite the maximum compressive stress at SDV1 located also near the minimum stress.

For SDV2 and SDV6, it is clear that these strain state are measured in the same direction as the loading. Where, it is shows a deformation in y direction. Therefore, the maximum stress for both elastic and plastic state, respectively, showing a tensile state, which is suitable with the loading direction. Whereas, the maximum tensile stress is located at the left and right side edge of the hole for the elastic and plastic state. For both state, the maximum compressive stress also located at the same region, which is at the upper and lower edge of the hole. By here, both elastic and plastic state have shared the same agreement with the maximum and minimum stress location, as well as the stress distribution behavior.

For SDV3 and SDV7, these strain state are measured in the out-of-plane direction, since the model is using a plane strain condition. Where here, a Poisson's effect is also observed,

since the stress state is showing the opposite behavior compared to SDV2 and SDV6. Where for instance in the upper and lower region, the stress state showing a tensile for SDV7 and SDV3, while for SDV2 and SDV6 showing a compressive state. This is clearly suitable with the Poisson's effect relation, where the material tends to expand in the out-of-plane direction when compressed in the loading direction, and vice versa.

For SDV4 and SDV8, these strain state are measured in shear direction. These can be seen that the maximum and minimum shear strain for both elastic and plastic state are located in the same region, which is at the upper left and upper right side edge of the hole, respectively. From this agreement, despite the shear strain distribution is still dominated by the elastic state, the material is already deformed plastically but in a smaller region which is shown in SDV8.

Finally, for SDV9, this shows the equivalent plastic strain (PEEQ) distribution, which is a scalar measure of the accumulated plastic deformation. Hence, it can be seen that the distribution is similar to SDV6, since the dominated plastic strain cause by the loading to the direction of y-axis. Here, it also shows the same location of the plastic strain, which is at the left and right side edge of the hole.

Conclusion

To sum up everything that have been analyzed and gathered in this study, here are some several key takeaways from this small case study:

1. **Mesh Convergence and Optimization:** The Mesh convergence study revealed that with the designed mesh configuration and shape dimension as in figure 2, a global and local mesh size of 0.8 mm and 0.4 mm respectively (mesh number 3) is sufficient to capture the Stress concentration Factor (K_t) accurately, according to the agreement of the effective K_t classical value that shows in figure 7.

2. **Symmetry Utilization:** By utilizing symmetry in both geometry and boundary conditions, a simplified model was proposed that significantly reduced computational cost and simulation time, while still accurately representing the full model's stress distribution, as shown in figure 9.

3. **Hardening Mechanisms:** The investigation of isotropic and kinematic hardening models under cyclic loading revealed distinct material responses for both mechanism, as well for the combined hardening. Isotropic shows a expansion of the yield surface, while kinematic shows a translation of the yield surface.

4. **UMAT Implementation:** The implementation of a J2 plasticity UMAT shows the exact results as the embedded J2 model in Abaqus, as shown in the true stress-strain curve comparison. This indicates the UMAT's capability to accurately model plasticity behavior.